Graphical Abstract

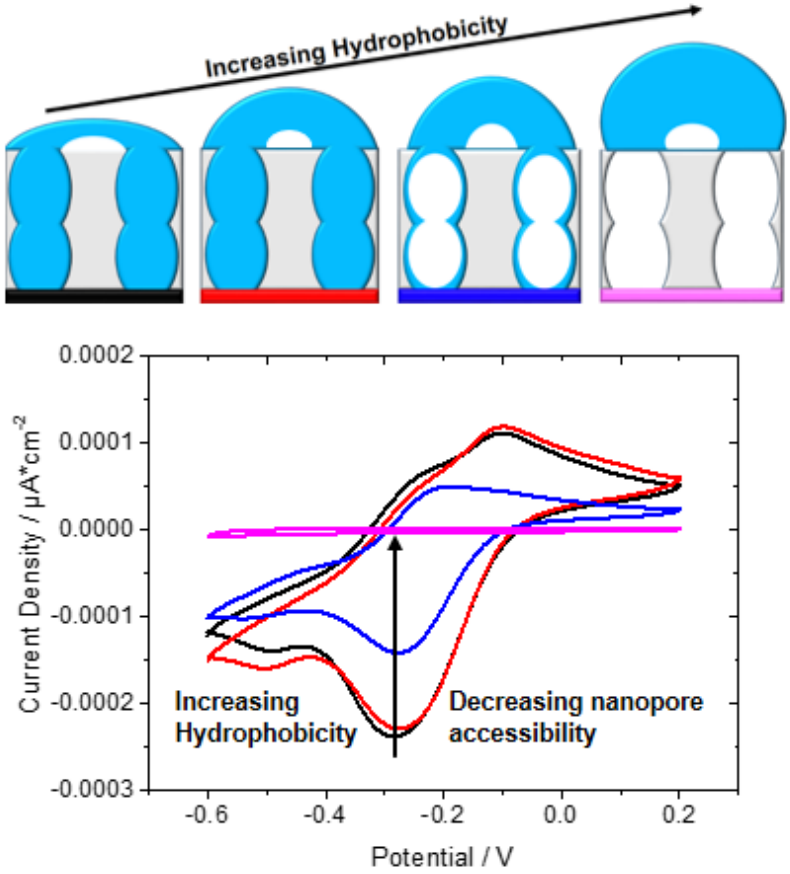

Insights into the interplay of wetting and transport in mesoporous silica films

*Adnan Khalil[a], Matthias Zimmermann[b], Alena K. Bell[c], Ulrike Kunz[d], Steffen Hardt[e], Hans-Joachim Kleebe[d], Robert W. Stark[c], Peter Stephan[b], Annette Andrieu-Brunsen[a]**

[a]Ernst-Berl-Institut für Technische und Makromolekulare Chemie, Technische Universität Darmstadt, Alarich-Weiss-Straße 8, 64287 Darmstadt, Germany

[b]Institut für Technische Thermodynamik, Technische Universität Darmstadt, Alarich-Weiss-Straße 10, 64287 Darmstadt, Germany

[c]Physics of surfaces, Technische Universität Darmstadt, Alarich-Weiss-Straße 16, 64287 Darmstadt, Germany

[d]Intitut für Angewandte Geowissenschaften, Technische Universität Darmstadt, Schnittspahnstraße 9, 64287 Darmstadt, Germany

[e]Nano- und Mikrofluidik, Technische Universität Darmstadt, Alarich-Weiss-Straße 10, 64287 Darmstadt, Germany

khalil@smartmem.tu-darmstadt.de zimmermann@ttd.tu-darmstadt.de

bell@pos.tu-darmstadt.de u.kunz@phm.tu-darmstadt.de

hardt@nmf.tu-darmstadt.de kleebe@geo.tu-darmstadt.de

stark@pos.tu-darmstadt.de pstephan@ttd.tu-darmstadt.de

Correspondence to A. Andrieu-Brunsen[a*]; Tel.: +49 6151 16-23742, *E-mail: andrieu-brunsen@smartmem.tu-darmstadt.de

Abstract

The understanding and design of wetting-transport and wetting-charge-transport interplay in nanometer-sized pores is a still not fully understood key step in improving nanopore transport-related applications. A control of mesopore wettability accompanied by pore filling and ionic mesopore accessibility analysis is expected to deliver major insights into this interplay of nanoscale pore wetting and transport.

For a systematic understanding, we demonstrate a gradual adjustment of nanopore ionic accessibility by gradually tuning silica nanopore wettability using chemical vapor phase deposition of 1H,1H,2H,2H-perfluorooctyl dimethylchlorosilane. The mutual influence of wetting on liquid imbibition, condensation, and molecular transport as well as on heat transfer were studied by ellipsometry, cyclic voltammetry and boiling experiments, respectively.

A multi-methodical analytic approach was used to directly couple wetting properties of mesoporous silica thin films to ionic mesopore accessibility allowing us to determine two different ion transport mechanisms based on three defined wetting regimes as well as a threshold hydrophobicity suppressing pore accessibility. Furthermore, boiling experiments showed a clear increase in nucleation site density upon changing the wettability of the mesoporous surfaces from hydrophilic to hydrophobic. Hence, these results provide insights into the complex interplay of pore wall functionalization, wetting, and charge-dependent nanopore properties.

Keywords: Mesoporous silica thin films, wettability, ionic transport, condensation, imbibition

Abbreviations: AFM, atomic force microscopy; AOI, angle of incidence; CA, contact angle; CV, cyclic voltammetry; ITO, indium tin oxide; PFODMCS, 1H,1H,2H,2H-perfluorooctyl dimethylchlorosilane; TEOS, tetraethoxysilane; RH, relative humidity; RT, room temperature; XPS, X-ray photoelectron spectroscopy

1. Introduction

Mesoporous inorganic materials are of great interest in many areas as nanoengineered structures.[1-2] Their combined properties such as controlled porosity, high flexibility and precision structure and surface functionalization provide the basis for materials with high adaptability to different applications, making them key components in catalysis, adsorption-based separation, boiling heat transfer, and future water purification concepts.[3-5] To adapt mesoporous material characteristics to specific applications, the concept of "hybrid organic–inorganic" nanocomposites has gained extraordinary attention since the 1980s.[6] By coupling organic molecules to an inorganic framework, tailoring of the inherited properties, such as hydrophilicity / hydrophobicity, polarity, and electronic activity, has been demonstrated.[7-9] To achieve molecular transport control, hybrid organic-inorganic thin films have been prepared by co-condensation or post-grafting steps to function as membranes with controlled and/or switchable permeability using thermo- and pH-responsive polymers[10] or photoresponsive azobenzene-containing organosilanes.[11-12] In the context of future water management, separation, sensing, and boiling, the wettability design of nanoscale pores represent an essential aspect e.g. porous ceramic membranes were tested for water desalination after hydrophobization by grafting fluorosilanes as a low surface free energy agent from solution.[13-14, 4]. To date, the interaction of water with nanoporous surfaces has been subject of various studies. Ceratti et al. illustrated that the liquid natural infiltration in nanoporous materials is governed by an interdependent mechanism of liquid infiltration by capillarity and evaporation, whereby the relative contribution of the driving force is determined by the porous structure.[15] Berli and co-workers deepened the understanding by describing spontaneous water adsorption-desorption oscillations at the imbibition front in mesoporous thin films which were strongly influenced by the structure of the mesoporous material.[16-17] Still, the influence of

wettability as well as the impact of the liquid imbibition on molecular transport has not been addressed to date, although it is known that wettability can be utilized to manipulate liquid and molecular transport e.g. in form of a hydrophobic gating.[18] For instance hydrophobic synthetic membranes initially expel water but can be wetted if other exterior forces, such as an electrostatic potential, are involved.[19] Both, Steinle et al.[20] and Holmes-Farley et al.[21] introduced ionizable groups onto inorganic nanopore (200 nm porediameter) walls or polymer films, respectively, by covalently attaching organic, pH-responsive molecules to the surface. By varying the pH value, a response in the wetting properties due to the strong influence of electrostatic interactions on wetting was achieved.[22] A similar approach was followed by Smirnov et al., who created a mixed monolayer of organic molecules in inorganic porous membranes, allowing a controlled flow of an aqueous solution in a pH range suitable for drug delivery.[23] In 2014, Huber and co-workers[24] showed that water infiltration in mesoporous gold structures is switchable by applying a potential. In summary, a clear effect of porous structure on water infiltration and subsequent water movement as well as of hydrophobization and water imbibition gating by the introduction of surface charges has been described. However, although wetting is omnipresent in both, technical processes and nature, and determines nanopore transport, the present studies are limited to either wetting or nonwetting states and controlled functionalization for pore diameters smaller than 10 nm allowing gradual control of functional density in confined space, and thus, rationally designing gradual wettability control is still challenging.[14, 25-26] Furthermore, no systematic studies have been performed which directly connect mesopore wettability together with water imbibition to ionic transport and the resulting transport mechanisms, to the best of our knowledge. Gradual tuning of wettability would open the door for advanced material design and a systematic investigation of wetting-pore characteristics – transport correlation. Further development of applications, such as

membrane-based water treatment or cooling by boiling, would significantly profit from gradual adjustment of the wetting properties in nanoporous structures.

In this study, a low surface free energy agent, 1H,1H,2H,2H-perfluorooctyl dimethylchlorosilane (PFODMCS), was used in an easy and fast procedure to gradually control hydrophobicity using time-dependent vapor phase deposition of PFODMCS on mesoporous silica pore walls with pore diameters of 6 – 8 nm. As a result, three wetting regimes in the nanoporous coatings or separation layers were observed and determined the ionic transport, water condensation, and boiling behavior. A threshold hydrophobicity was determined, at which point the mesopores are closed by wetting but can be opened by electrostatic attraction. By correlating this gradual wetting control to ionic transport, water imbibition, water condensation, and boiling characteristics, we enhance our understanding of how to optimize applications related to nanoporous materials.

2. Materials and methods

Pluronic® F127 was purchased from Sigma-Aldrich. Tetraethoxysilane (TEOS) and 1H,1H,2H,2H-perfluorooctyl dimethylchlorosilane (PFODMCS) were purchased from Alfa Aesar. Ethanol (absolute) was purchased from Merck Millipore. All chemicals were used as received unless otherwise noted.

2.1. Mesoporous Thin Film Preparation

Mesoporous silica thin films were prepared by sol-gel chemistry using Pluronic® F127 as a template in the presence of TEOS as a precursor. The precursor solution contained the following molar ratios: 1 TEOS:0.0075 F127:10 H2O:40 ethanol:0.28 HCl (37 %). The solution was stirred overnight before the dip-coating step to produce thin films with a withdrawal speed of 2 mm/s. The thin films were deposited on glass, indium tin oxide (ITO, Delta Technologies), or silicon wafer (Si-Mat) substrates at a relative humidity (RH) of ~50 % and a temperature of ~23°C. Freshly deposited films were kept under these climate conditions for at least 1 h before being thermally treated. The films undergo two consecutive stabilization steps by heating to 60°C in 10 min and holding this temperature for 1 h. Afterwards, the temperature was increased to 130°C in 10 min and again held for 1 h. Then, the temperature was increased to 350°C at a rate of 1°C/min and held for 2 h to burn off the organic template. Finally, the samples were rinsed with ethanol leading to films with thicknesses of ~130-250 nm and a porosity of ~50 % measured by ellipsometry.[27]

2.2. Vapor-phase deposition of 1H,1H,2H,2H-perfluorooctyl dimethylchlorosilane

Vapor-phase deposition of 1H,1H,2H,2H-perfluorooctyl dimethylchlorosilane (PFODMCS) was performed in a vacuum chamber with a volume of 1 L at room temperature. First, the samples were cleaned with ethanol and dried with pressurized nitrogen before being placed in the reaction chamber. The chamber containing the samples was alternatingly evacuated and flushed with gaseous nitrogen three times before 20 µl of PFODMCS was placed into the chamber in a counterflow of nitrogen. Afterwards, a reduced pressure of 40 mbar was applied to the chamber and maintained for different intervals of time. Finally, the samples were rinsed and extracted with ethanol and toluene before being stored under ambient conditions.

2.3. Contact Angle

Macroscopic Young contact angles (CAs) were measured with an OCA 35 device by DataPhysics Instruments using the SCA 4.5.2 software and the sessile drop method under standard atmosphere (T = 23°C, RH = 50 %). A drop volume of 2 µl was used, and the CA value was obtained by fitting the droplet shape using the approximation algorithm of the SCA software. Dynamic CA was measured by increasing and decreasing the droplet volume from 2 µl to 10 µl with a dosing speed of 0.2 µl/s. Simultaneously a video was recorded and later analyzed for the dynamic CA by the SCA 4.5.2 software.

2.4. Ellipsometry

Ellipsometry was applied for reflecting silicon wafers (Si-Mat) using a Nanofilm Model EP3 imaging ellipsometer to determine the film thicknesses and refractive indices of the mesoporous thin films before and after functionalization. Therefore, one zone angle of incidence (AOI) variation measurements were captured between 38° and 68° in steps of 2° with a laser of 658 nm. The apparent film thicknesses and refractive indices were calculated from the measured

ellipsometric angles Ψ and Δ, using the EP4 analysis software supplied with the instrument. The measured data were fitted with a one-layer box model. The fitting range covers a film thickness from 100 to 250 nm and a refractive index range of 1 to 1.5. All films were measured at three identically marked positions before and after functionalization. Changes were calculated for each specific position followed by the mean value and error determination. To determine the porosity from the refractive indices, the Brüggemann effective medium approximation was used.[28] Standard ellipsometry – measurements were performed in air at a RH of 20 % or under water. To observe the adsorption behavior of water in the mesoporous film, the RH-dependent change in the refractive index was monitored using a humidity control (SolGelWay) according to Boissiere et al.[27]

2.5. Cyclic voltammetry (CV)

CV measurements were performed using a Metrohm Autolab PGSTAT302N potentiostat in combination with the Nova 1.9 software for collection of the data. The three-electrode set up consisted of an Ag/AgCl reference electrode, a graphite counter electrode and mesoporous thin films on a conductive ITO surface (Delta Technologies) as the working electrode (exposed area 0.21 cm^2). Ionic permselectivity was observed by using two different probe molecules with a concentration of 1 mM, i.e., the positively charged $[Ru(NH_3)_6]^{2+/3+}$ and the negatively charged $[Fe(CN)_6]^{4-/3-}$, in a 100 mM aqueous KCl solution, resulting in an electronic double layer (EDL) of ~ 1 nm. The cyclic voltammograms were obtained at different scan rates in the following order: 200 $mV*s^{-1}$ / 100 $mV*s^{-1}$ / 25 $mV*s^{-1}$ / 300 $mV*s^{-1}$ / 1000 $mV*s^{-1}$/ 200 $mV*s^{-1}$. The cyclic voltammograms in the text of the manuscript correspond to 100 $mV*s^{-1}$ if not specifically noted. Measurements were performed under acidic (pH = 3) and basic (pH = 9) conditions, which used 1 N HCl and NaOH, respectively.

2.6. X-ray photoelectron spectroscopy (XPS).

XPS was recorded using a Surface Science Laboratories SSX-100 X-ray photoelectron spectrometer equipped with a monochromatic Al Kα X-ray source (100 W). The X-ray spot size was 250-1000 µm. The binding energy scale of the system was calibrated using Au $4f_{7/2}$ = 84 eV and Cu $2p_{3/2}$ = 932.67 eV signals from foil samples. A Shirley background was subtracted from all spectra. Peak fitting was performed with Casa XPS using 70/30 Gaussian-Lorentzian product functions. Atomic ratios were determined from the integral intensities of the signals, which were corrected by empirically derived sensitivity factors.

2.7. Atomic force microscopy (AFM)

A Dimension ICON (Bruker AXS, Santa Barbara, CA, USA) was used in intermittent contact mode for measurements of the height profile to later extract the roughness of the characterized silica films. Two different kinds of cantilevers were used. Both cantilevers were calibrated by the thermal noise method.[29] For an unmodified mesoporous silica film, an RFESP-75 cantilever (Bruker AFM Probes, Camarillo, CA, USA) with a force constant of 1.75 N/m was used, while for a hydrophobic mesoporous silica film, a ZEIHR cantilever (Nano And More, Wetzlar, Germany) with a force constant of 5.9 N/m was used. For the measurements, the amplitude setpoint was set to 46 % with a free amplitude of 41 nm (RFESP-75 cantilever) and 42 nm (ZEIHR cantilever). The surface topography was analyzed by using the AFM software (NanoScope Analysis 1.8). The area root mean square roughness (S_q), which is the standard deviation of heights within the image, was used to compare the surfaces.[30]

2.8. Boiling

To investigate the influence of the wettability of the mesoporous silica thin films on the nucleate boiling performance, tests using a self-built boiling chamber were performed. Mesoporous silica

films were deposited by dip coating onto polished aluminum substrates, which were 2 cm in diameter and 8 mm in height. DI-water was used as the boiling fluid, and the boiling tests were performed at 70 mbar. Before starting the experiments, water was degassed for 3 hours. The time-resolved boiling behavior was observed by a high-speed black and white camera (*Mikrotron* MotionBLITZ EoSens Cube 7). A hydrophilic, unfunctionalized reference mesoporous silica film (CA < 20°) and a functionalized hydrophobic mesoporous film (CA > 90°) were investigated at various heat fluxes.

3. Results and discussion

3.1. Gradual tuning of wetting properties

Mesoporous silica films on different supporting substrates (glass, Si-Wafer, ITO) were obtained via sol-gel synthesis and evaporation-induced self-assembly utilizing a sol containing TEOS as the silica precursor and the block-copolymer template Pluronic® F127. In agreement with previous studies, [31-33] ~170 nm thick mesoporous silica films with a pore diameter of approximately 6-8 nm and a neck diameter of 2-3 nm were obtained as supported by transmission electron microscopy images (details in Supporting Information **Figure S1**). The surface active hydroxyl groups, which are able to perform condensation reactions as pictured in **Figure 1 a,** are used for the PFODMCS functionalization and gradual wetting design.

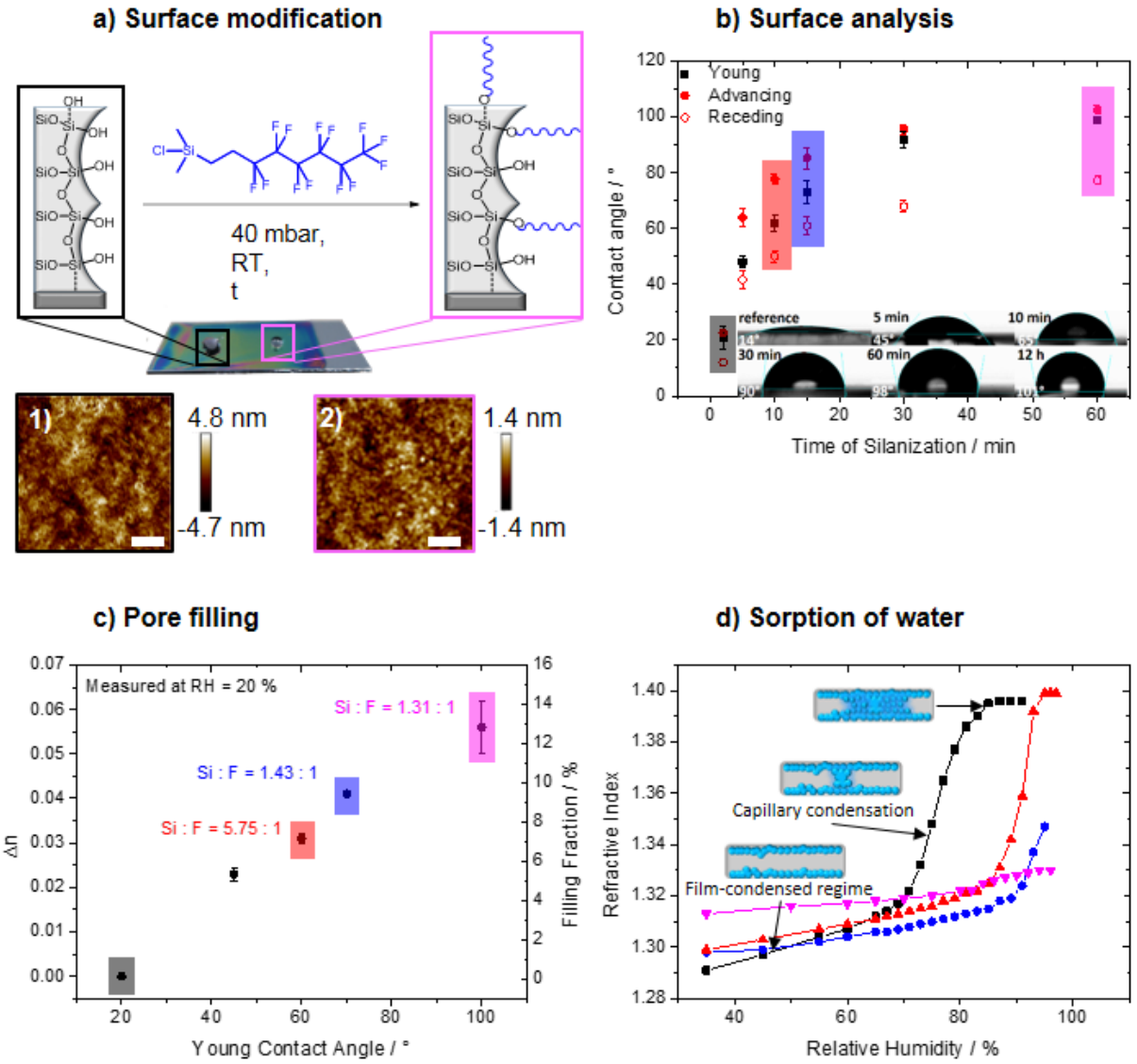

Figure 1. a) Schematic view of the time-dependent mesoporous silica thin film functionalization by PFODMCS vapor phase deposition at room temperature (RT) plus corresponding AFM images before 1) and after functionalization for 60 min 2 (scale bar = 200 nm). **b)** Influence on the wetting properties as a function of the functionalization time (t), as reflected by the macroscopic Young contact angles (CAs). **c)** Variation of pore filling with silanization time as reflected by the refractive index and pore filling fraction as well as by the Si:F ratio measured by XPS and **d)** its influence on the sorption behavior of water as reflected by the refractive index in dependence of

the increasing relative humidity (black: reference., red: CA ~ 60°, blue: CA ~ 70°, magenta: CA ~ 100°). For clarity, only the adsorption curves are pictured here. For the full adsorption-desorption curves, see the SI (**Figure S4**).

Ellipsometry results of unfunctionalized mesoporous films (**Figure 1 c**) indicate a porosity of ~50 vol%. Upon functionalization with PFODMCS, the porosity decreases (**Figure 1 c** and **d**) as the CA increases with functionalization time (**Figure 1 b** black). However, even after reaching the maximum hydrophobization (CA ~ 100°), the mesopore filling fraction reaches only approximately 14 %, meaning the pores are not sterically blocked. In agreement with the ellipsometry and the decreasing free pore volume with increasing functionalization time results, the XPS measurements (see SI **Table S3**) show an increase in the fluorine (at ~ 689 eV) to silicon (at ~ 103 eV) ratio from 0.18 after functionalization for 2 min (CA < 70°) up to 0.74 for mesoporous films functionalized for 1 h (CA ~ 100°), indicating a functional density of approximately 1 PFODMCS per 17 Si. Thereby, the films show low root mean square surface roughness in the range of S_q = .36 nm (before functionalization) and S_q = 0.39 nm (after 60 min of functionalization) over the entire scan area (**Figure 1 a**). Further AFM data, including cross-sections, are presented in the SI (**Figure S7 – S8**). The resulting CAs are depicted in **Figure 1 b**. With the increasing reaction time, an increasing CA is observed due to increasing surface functionalization and decreasing surface energy of the naturally hydrophilic silica material. Therefore, the mesoporous film wettability is gradually adjusted from hydrophilic (CA < 20°) to hydrophobic (CA ~ 100°) within 60 min of functionalization time in a fast and easy manner. This extends the range of application for perfluorinated silanes, as otherwise they are only used to achieve high levels of surface hydrophobicity.[13, 34-38] Interestingly, a higher CA, reaching the

superhydrophobic regime (CA ≥ 150°), was not observed raising the question of present wetting states.

To investigate the effect of mesopore wall hydrophobization on wetting and water condensation inside the mesoporous film, water porosimetry[27] was investigated using ellipsometry. Therefore, two regimes of sorption in nanoporous media are distinguished: the film-condensed regime and the capillary condensation. The latter describes liquid-vapor transition for the confined state.[39] In the film-condensed regime, molecules form a thin film on the pore walls until a critical vapor pressure is reached. Beyond the critical vapor pressure, capillary condensation begins by forming liquid bridges. With the addition of more molecules, the menisci move forward to the pore ends until the pore space is completely filled.[39] The process of water condensation in the mesoporous film as detected by ellipsometry is evaluated using Brüggemann's effective medium theory,[28] i.e., monitoring the refractive index increase with increasing partial pressure and thus substitution of air (n = 1) by water (n = 1.33). A clear influence of the surface functionalization on water adsorption is observed (**Figure 1 d**). For clarity, only the adsorption curves of water on the mesoporous thin films are shown. Complete adsorption-desorption curves are pictured in the supporting information (**Figure S4**). For the unmodified reference material, a type IV hysteresis curve is observed, which is typical of mesopores with a pore diameter > 4 nm (**Figure S4 a**).[40] Upon functionalization resulting in a macroscopic static CA below 70°, the hysteresis seems to turn into type V (**Figure S4 b)**, which is typical for micropores or for the adsorption of water into a hydrophobic material. Therefore, capillary condensation occurs over a smaller range of relative humidity in comparison to the hydrophilic unmodified reference film, as reflected by a steeper increase in the refractive index, which is also presented in **Figure 1 d** (red). Due to functionalization, hysteresis increases, indicating more pore blocking (a combination of pore

parameters such as narrow bottle necks and functionalization). Upon further increasing the functionalization time and thus functional density and CA, capillary condensation is not complete up to a relative humidity of 97 % (CA ~ 70°, **Figure 1 d** blue) or is completely prevented (CA ~ 100°, **Figure 1 d** magenta). In addition, capillary condensation is shifted to a higher relative humidity (RH) with the increasing degree of functionalization and thus the CA shifts from 70 % for a CA of 20° (**Figure 1 d** black) to 90 % for a CA of 60° (**Figure 1 d** red). In the case of CA ~ 70° (**Figure 1 d** blue), the results give rise to the question of whether the capillary condensation of water is prevented due to the degree of functionalization or the limits of the experimental setup (highest adjustable RH possible is 97 %). Therefore, additional ellipsometry measurements under liquid water were performed (see SI **Table S2**). In the following **Figure 2**, a comparison of refractive indices is made for different degrees of functionalization, as indicated by the CA, under different atmospheric conditions of dry air (RH = 20 %), wet air (RH > 90 %) and liquid water.

The refractive index of water-filled mesoporous silica thin films with a porosity of 50 % should be between ~1.390-1.400, i.e., between the refractive index of water (n=1.33) and nonporous silica (n=1.455), as estimated from the effective medium theory.

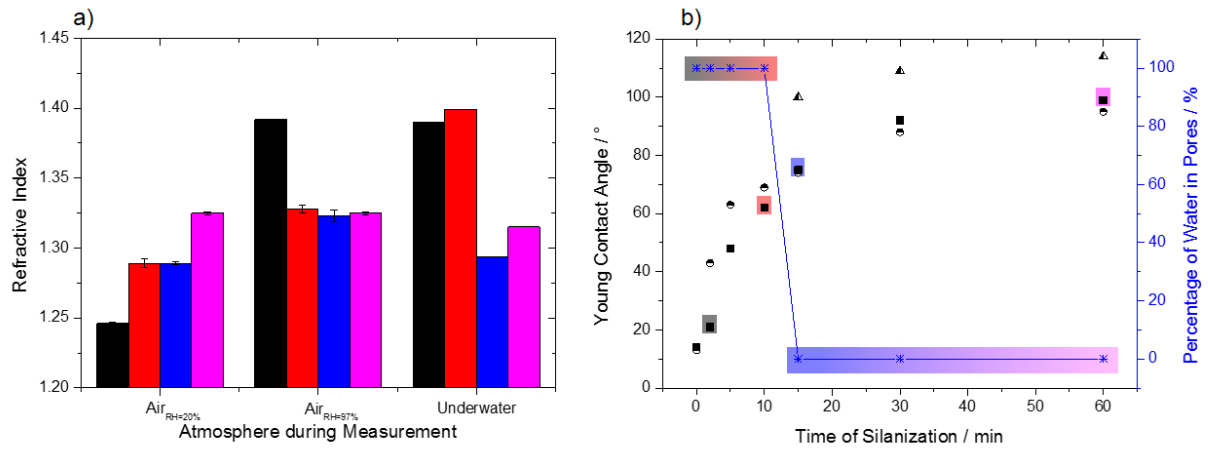

Figure 2. a) Refractive index determined by ellipsometry for an unmodified reference sample (black), a mesoporous film showing a CA below 70° (red), a mesoporous film showing a CA of ~70° (blue) and a hydrophobic mesoporous film with a CA significantly higher than 70° (magenta). The measurements were performed under different atmospheres, namely, dry air ($Air_{RH=20\%}$), wet air ($Air_{RH=97\%}$) and liquid water (underwater). **b)** Experimental CAs for mesoporous (black filled squares) and nonporous dense, planar silica films (black half-filled circles) in comparison to the theoretically calculated CAs according to Cassie-Baxter relation for gas-filled pores (black half-filled triangles) as well as percentages of water in pores under a liquid water atmosphere (blue stars).

The refractive index of the reference material as well as that of the mesoporous thin films with a CA below 70° increases in wet air and/or under water due to water condensation or water imbibition, respectively. Interestingly, a CA of 70° (advancing CA of 90°) represents a kind of transition state with respect to water infiltration and water adsorption. It is known from the literature that confined water, especially in hydrophobic gaps, behaves differently from bulk water. It can spontaneously evaporate in hydrophobic gaps < 10 nm.[18, 41-42] Mesoporous films with a CA of ~ 70° (advancing CA ~ 90°) seem to present a configuration for which the degree of

functionalization starts to be sufficiently high to induce spontaneous evaporation and hence prevent complete capillary condensation, especially in narrower regions of the porous network such as bottlenecks and pore interconnections. At a wetting transition state Yang et al. describes partly filled pores of anodic aluminum oxide surfaces while exposed to liquid water.[43] Under the applied conditions partly filled pores are only observed at high relative humidity (97 %) but not in contact with liquid water under ambient conditions. As shown in in **Figure 1 d** (blue), capillary condensation seems to initiate for a CA of ~ 70°. This implies the completion of the film condensation regime. In contact with liquid water, however, the refractive index is comparable to that measured in dry air for such a mesoporous film with a CA of ~ 70°, which indicates that the vapor pressure below liquid water under ambient conditions and functionalized mesoporous films with a CA of ~ 70° is not sufficient to induce water condensation and water pore filling. A less hydrophilic sample with a CA > 70° shows no significant changes at all in the refractive index, even at a RH of 97 %. Taking all observations together, CA < 70° results in water-filled mesopores if in contact with liquid water at ambient temperature, whereas a CA > 70° results in air-filled pores under these conditions. For CA allowing water infiltration into the mesopores (CA < 70°), a slightly lower CA for mesoporous films compared to that of planar dense silica films is observed (**Figure 2 b** red vs. black). Under conditions with CA > 70°, corresponding to air-filled mesopores, slightly higher CA values are observed for mesoporous films than for planar dense films. Interestingly, the maximum CA achieved upon functionalization does not exceed ~ 100° (CA of ~94° on a nonporous material (**Figure S3**)) indicating absence of surface structure on nonporous materials after functionalization.

The rather sharp transition between water-filled pores and air-filled pores at a CA of ~ 70° suggests using the classic Wenzel[44] and Cassie-Baxter[45] models to study the effects of roughness

on wetting. Here, the term "roughness" refers to the increase of surface area due to the large-aspect ratio mesopores. Estimating a solid area fraction of 35 % from TEM images (**Figure S1 – S2**) and based on the CA observed under identical functionalization conditions for planar, nonporous silica films (**Figure S3**), the Cassie-Baxter theory would predict a higher CA than found in the experiments (**Figure 2 b**). Owing to the large aspect ratio of the pores, the Wenzel model, however, predicts that the CA sharply drops to values close to zero as soon as the pores get filled with water (data not shown), at variance with the results of **Figure 2 b** for CA values < 70°.

To qualitatively explain the discrepancies between the experimental data and the classic models of wetting on rough surfaces, we first focus on the Wenzel model. Input parameters of the model are the solid-gas and solid-liquid interfacial tensions, among others. The solid-gas interfacial tension, for example, measures the excess potential energy of atoms at the surface relative to atoms in the bulk of the solid. The standard values for interfacial tensions are values for flat surfaces bounded by an infinitely extended second medium. However, in pores with diameters between 3 and 10 nm, the atoms at the surface of a nanopore also interact with atoms at the opposite side of the pore wall. For attractive interactions this reduces the interfacial tension of this surface compared to a flat surface. Likewise, the gas-liquid interfaces that need to be considered in the Cassie-Baxter model are nanoscopic interfaces with properties different from macroscopic ones. Owing to the close proximity of solid material for all molecules at a gas-liquid interface, its effective surface tension is lower than that of a macroscopic interface. In both the Wenzel and the Cassie-Baxter model, these proximity effects make it necessary to work with effective interfacial tensions that are lower than their classic counterparts. This qualitatively explains why in **Figure 2 b** the classic Cassie-Baxter model overpredicts the CA for values > 70°, while the classic Wenzel model underpredicts it for values < 70°.

3.2. Influence of wetting properties on ionic mesopore accessibility

Wetting, water condensation, and water imbibition are parameters that strongly determine molecular transport phenomena in mesoporous materials, which are performance limiting in many applications, such as water management. Therefore, investigating pH-dependent ionic transport into mesopores as a function of the CA and underwater conditions has been performed using cyclic voltammetry. In the case of redox-active probe molecules reaching the electrode below the mesoporous film, mesopores are filled with at least a water layer through which the transport of solvated ions can occur, as schematically depicted in **Figure 3 a**.

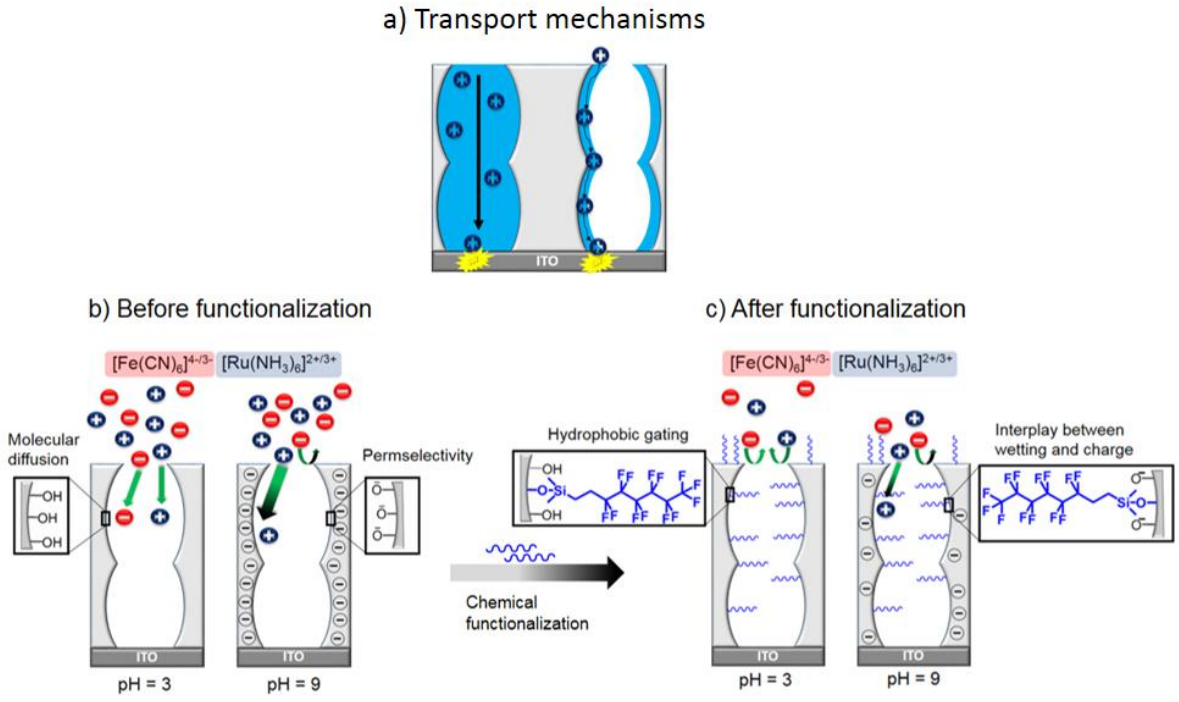

Figure 3. a) Two possibilities of transport for ions through mesopores: diffusion through completely water-filled mesopores (left) and transport along a condensed water film on pore walls (right). Detection occurs on a conductive supporting substrate. **b) +c)** Schematic depiction of the pH-dependent ionic transport occurring in the mesoporous thin films before **b)** and after **c)** functionalization with PFODMCS at different pH values. **b)** At pH = 3, the mesopores are neutral,

and thus, no exclusion of ionic species is expected; whereas at pH = 9, negatively charged mesopores and ion permselective transport with favored transport of cations are expected. **c)** At pH = 3, neutral mesopores functionalized with hydrophobic silanes (PFODMCS) are expected to show charge-independent behavior, increasing the exclusion of both test molecules depending on the degree of functionalization and thus on the nanopore wetting (contact angle). At pH = 9, for negatively charged mesopores with hydrophobic silanes (PFODMCS), an exclusion of both test molecules is observed if a threshold hydrophobicity is exceeded. At a threshold hydrophobicity, attractive electrostatic interactions allow the transport of countercharged test molecules.

Ionic transport characterization using cyclic voltammetry allows us to consider not only wetting but also the effect of the acidic silanol groups present at the silica mesopore walls, as well as the influence of the resulting pH-dependent charges, which have been neglected in the discussion above regarding wetting and water condensation. In general, these silanol-based charges induce an ionic permselectivity of silica mesopores, enabling the mesoporous structure to selectively transport or exclude ions independent of their charge. To manipulate this inherent ionic permselectivity, the wettability of the mesoporous films, the pH value of the probe molecule solution in contact with the mesoporous films, and the redox-active probe molecules are systematically varied. The ionic transport is examined on mesoporous films supported on indium tin oxide (ITO) electrodes using the anionic and cationic electro-active probe molecules, $[Fe(CN)_6]^{4-/3-}$ and $[Ru(NH_3)_6]^{2+/3+}$. In **Figure 3**, the expected ionic transport behavior before (**Figure 3 b**) and after functionalization (**Figure 3 c**) for acidic and basic pH values is schematically depicted.

Before functionalization, at an acidic pH value below three, a similar maximum peak current density and thus a similar mesopore accessibility for the negatively charged $[Fe(CN)_6]^{4-/3-}$ and the

positively charged $[Ru(NH_3)]_6^{2+/3+}$ redox probe molecules are expected because the mesopore walls are not charged. However, at an alkaline pH value of nine, permselective ionic transport due to electrostatic attraction of $[Ru(NH_3)]_6^{2+/3+}$ and electrostatic repulsion of $Fe(CN)_6]^{4-/3-}$ and pore sizes within the range of the Debye screening layer should occur. Therefore, functionalization with hydrophobic silanes (PFODMCS) should result in a functionalization time (functionalization degree)-dependent increase in critical infiltration pressure for water. Hence, neutral mesopores at pH values below three are expected to show charge-independent increasing exclusion of both probe molecules. By adjusting the pH value to nine and therefore introducing the negative charges of the remaining silanol groups to the mesopore wall, the ionic permselective transport described for unfunctionalized mesopores is expected to be additionally influenced by the wetting-controlled water infiltration. An exclusion of both redox probe molecules, independent of their charge, is expected in the case the threshold hydrophobicity is exceeded. Exclusion due to hydrophobic gating is expected at CA ≥ 90° according to the Laplace equation.[23]

The first characterization of mesopore accessibility using cyclic voltammetry (see SI **Figure S5**) on samples showing a CA of ~ 20° (unfunctionalized reference), CA ~ 40°, CA ~ 90°, and CA > 100° shows the expected behavior for hydrophilic and hydrophobic (CA ~100°) mesoporous films but, in accordance with the above discussed results, also suggest a threshold hydrophobicity at a CA below 90°. At this threshold, the hydrophobicity wetting-based charge-independent probe molecule exclusion at acidic pH (neutral pore wall) is observed, while at basic pH, the electrostatic attraction between the mesopore walls and the positively charged $[Ru(NH_3)_6]^{2+/3+}$ results in probe molecule transport, indicating that electrostatic attraction is able to overcome wetting-based probe molecules and water exclusion for threshold wettability without fully filling the pores, most likely based on a condensed film at the mesopore wall. Further systematic cyclic voltammetry

characterization (**Figure 4**) confirmed the expected wetting and pH-dependent ionic mesopore accessibility and revealed a threshold hydrophobicity of ~70°.

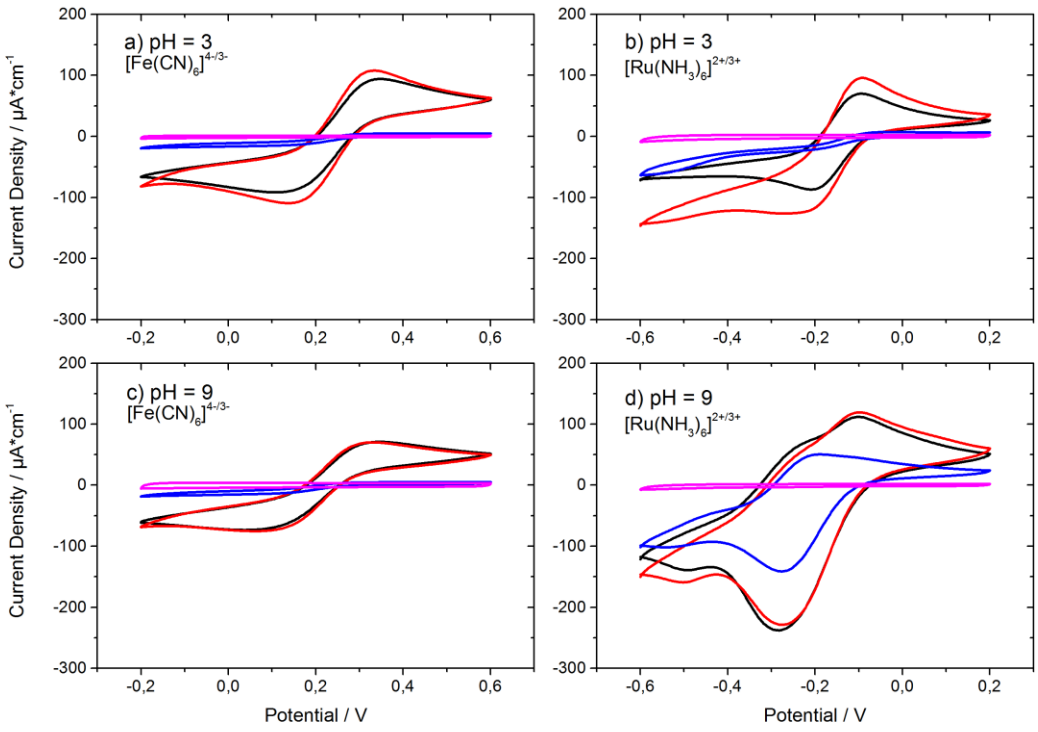

Figure 4. Cyclic voltammograms displaying the ionic transport of the positively charged $[Ru(NH_3)_6]^{2+/3+}$ and the negatively charged $[Fe(CN)_6]^{4-/3-}$ through mesoporous thin films with different wetting properties (static CA ~ 20° (black), CA ~ 45° (red), CA ~ 70° (blue), and CA ~ 80° (pink)) for a pH value a) + b) pH = 3 and c) + d) pH = 9. Scan rate: 100 mV/s. Electrolyte: 1 mM redox compound in 0.1 M KCl (aq).

In more detail, for the reference, the highest maximum peak current density is observed for $[Ru(NH_3)_6]^{2+/3+}$ at pH = 9 due to electrostatic attraction (220 µA/cm^2), whereas electrostatic

repulsion of the anionic $[Fe(CN)_6]^{4-/3-}$ caused its electrostatic exclusion, resulting in a maximum peak current density of 70 µA/cm^2. For neutrally charged mesoporous films at a pH value of three, similar current densities of 90 – 100 µA/cm^2 for both probe molecules are detected. After functionalization by chemical vapor phase deposition of PFODMCS resulting in a CA of ~ 40°, only minor differences to the reference are noticed since the degree of functionalization is relatively low and the residual silanol functional groups at the mesopore wall still dominate the overall pore accessibility. However, further hydrophobization has a significant effect on the ionic mesopore accessibility for both redox probe molecules. Reaching a CA of ~ 70°, a threshold hydrophobicity is observed at which only the positively charged $[Ru(NH_3)]_6^{2+/3+}$ at an alkaline pH value is able to move through the mesoporous network and reach the electrode to be detected. Under acidic conditions, $[Ru(NH_3)_6]^{2+/3+}$ is excluded from the mesopores as well as negatively charged $[Fe(CN)_6]^{4-/3-}$, which is excluded under both acidic and alkaline conditions. For even further hydrophobized mesoporous films (Young's CA ~ 80-100°), completely inaccessible mesopores are obtained. Interestingly, the blue curve in **Figure 4 d** shows a changing shape of the cyclic voltammograms. While more hydrophilic mesoporous films exhibit a maximum peak current density at -0.09 V, the mesoporous film with a CA of ~ 70° shows a maximum at -0.22 V. In this potential region, the reference sample as well as the slightly modified sample (CA ~ 40°) display a shoulder in the current-voltage curves. This shoulder usually represents accumulated target analyte due to interacting with the porous material before its subsequent detection at the working electrode.[46] Considering the water-adsorption data and underwater ellipsometry results, which displayed incomplete capillary condensation for a CA of approximately 70° and air-filled pores for underwater conditions at ambient temperature (**Figure 1 d**, **Table S2**), the ionic transport at the threshold-hydrophobicity level around a CA of 70° is dominated by complex interactions of

the analyte molecules with the pore walls and probably a thin water film at the pore wall, whereas in the less- or unmodified mesopores with CA < 70°, the probe molecules can diffuse through the water-filled system (**Figure 3 a**). The observed air-filled pores for a CA of > 70° and the deviation from the theoretically expected Cassie-Baxter contact angle also support the formation of a thin water film at the pore wall, allowing electrostatically attracted molecules to pass along the pore wall to the electrode below the film (**Figure 3 a**).

Further modified mesopores (CA > 80°) did not allow any kind of transport of solvated ions because liquid water did not enter the pores at all. The combination of droplet analysis, ellipsometry, and cyclic voltammetry expands the understanding of the wetting – molecular transport interplay in mesoporous films and the role of wetting transitions. This is of particular importance for surface science and related applications such as sensing and molecular separation processes, since it shows how specific the combination of charge and wetting can enhance selectivity.

3.3. Influence of wetting properties on nucleate boiling

Related to further areas of application, nanostructured surfaces are known to improve the nucleate boiling heat transfer performance significantly.[47-49] Nucleate boiling is a viable option for cooling microelectronics due to the very high heat transfer coefficients. The heat transfer coefficient typically increases with increasing heat flux until a critical (maximum) heat flux is reached. This increase is closely related to the density of active nucleation sites on the boiling surface. The higher the nucleation site density is, the higher the heat transfer coefficient. The nucleation site density is typically higher on a nanostructured surface than a smooth surface, and it is higher on a hydrophobic surface than a hydrophilic surface. Smaller and more numerous bubbles can be

observed. However, the hydrophobicity typically reduces the critical heat flux because the rewetting of dry spots is aggravated.[50-51]

Capillary wicking effects in turn can facilitate rewetting.[52] To investigate the influence of mesoporous silica films with varying wettability on the nucleate boiling performance, boiling experiments with pure water in a pure vapor atmosphere were performed. The boiling surfaces are coated with silica films and superheated compared to the saturation temperature of the fluid. The boiling behavior was observed by a high-speed black and white camera. **Figure 5** shows the images of the growing vapor bubbles on the hydrophilic (a) and hydrophobic (b) surface for various heat fluxes.

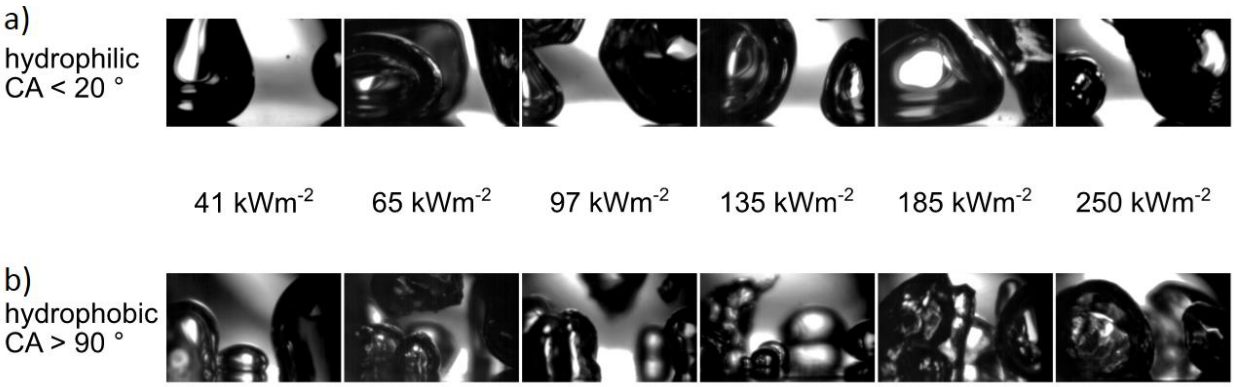

Figure 5. Images of growing vapor bubbles during nucleate boiling on a) a hydrophilic and b) a hydrophobic mesoporous silica thin film.

As expected, the bubbles on the hydrophilic mesoporous surfaces are much larger and less abundant than those on the hydrophobic mesoporous surface. The bubbles depart from the superheated surface with a lower frequency. The bubbles on the hydrophobic mesoporous surface are smaller and more numerous and depend on a higher frequency. Thus, higher heat transfer coefficients can be expected for the hydrophobic mesoporous surface[51]. This observation can be explained as follows: mesopores act as small cavities where the nucleation process is initiated.

Hydrophobic pores are activated more easily, thus increasing the nucleation site density, and they tend to facilitate vapor/gas entrapment during the bubble detachment process and thereby subsequent bubble growth.

4. Conclusion

In summary, the wetting properties of mesoporous silica thin films can be gradually tuned without blocking the mesopores by means of short reaction time vapor phase deposition of perfluorinated silanes in a much more sensitive way than described in literature.[14, 38, 53] The degree of hydrophilicity/hydrophobicity has a significant impact on mesoporous film wetting, water sorption, ionic pore accessibility, and heat transfer properties. Macroscopically, three wetting regimes define the mesoporous materials performance. In the hydrophilic regime (CA < 70°), the pores are fully wetted by water and are accessible to small ions, whereas in the hydrophobic regime (CA >70°), water is expelled and unable to condense in the mesopores. The measured CA for mesoporous films is slightly lower than that for identically functionalized planar surfaces for hydrophilic, wetted films and slightly higher for hydrophobic air-filled mesoporous films, although the measured CA for hydrophobic films is slightly lower than the theoretically expected CA based on Cassie-Baxter theory.[45] This is related to the nanoscopically confined structure, which is assumed to cause a decrease of the effective interfacial tension. At the transition between water-filled and air-filled pores (threshold hydrophobicity), air-filled mesopores are observed even while in contact with liquid water. Thus at this threshold hydrophobicity, close to the water imbibition transition, mesopores are not accessible for probe molecules. Interestingly, they can be electrostatically opened for positively charged ions at basic pH, as shown by cyclic voltammetry. This pore opening is probably due to a thin water film generated at the mesopore wall by

condensation becoming possible due to the change in pore wall wettability. This correlation between wetting and molecular transport is a separation and sensing technology relevant extension to literature studies describing the imbibition of water in spatially confined mesopores being dominated by liquid infiltration and condensation and evaporation at the same time.[15-17] This insight into the interplay of mesopore wetting and charge with transport mechanisms has been possible based on the combination of ellipsometry under water and at different water vapor pressures together with cyclic voltammetry and contact angle measurements. As these observations are highly relevant for technologies, such as future water management, molecular separation, water condensation, membrane distillation, and cooling by boiling, it is demonstrated that the hydrophobization of mesopores induces an increasing nucleation site density during boiling, leading to increased heat transfer coefficients. Considering the wide field of possible applications of nanostructured surfaces, the presented results enable the synthesis and characterization of multiple materials with designed structure and wettability.

Acknowledgements

We kindly acknowledge the financial support by the German Research Foundation (DFG) within the Collaborative Research Centre 1194 “Interaction between Transport and Wetting Processes”, Project <C04, C02, A07>. In addition, the authors wish to thank Karl Kopp and Prof. Hess for X-ray photoelectron Spectroscopy.

References

1. Kresge, C.; Leonowicz, M.; Roth, W. J.; Vartuli, J.; Beck, J., Ordered mesoporous molecular sieves synthesized by a liquid-crystal template mechanism. *nature* **1992,** *359* (6397), 710.
2. Ozin, G. A.; Hou, K.; Lotsch, B. V.; Cademartiri, L.; Puzzo, D. P.; Scotognella, F.; Ghadimi, A.; Thomson, J., Nanofabrication by self-assembly. *Materials Today* **2009,** *12* (5), 12-23.
3. Lee, C. Y.; Bhuiya, M. M. H.; Kim, K. J., Pool boiling heat transfer with nano-porous surface. *International Journal of Heat and Mass Transfer* **2010,** *53* (19-20), 4274-4279.
4. Li, R.; Zhang, L.; Wang, P., Rational design of nanomaterials for water treatment. *Nanoscale* **2015,** *7* (41), 17167-17194.
5. Soler-Illia, G. J.; Azzaroni, O., Multifunctional hybrids by combining ordered mesoporous materials and macromolecular building blocks. *Chemical Society Reviews* **2011,** *40* (2), 1107-1150.
6. Nicole, L.; Boissière, C.; Grosso, D.; Quach, A.; Sanchez, C., Mesostructured hybrid organic–inorganic thin films. *Journal of Materials Chemistry* **2005,** *15* (35-36), 3598-3627.
7. Moller, K.; Bein, T., Inclusion chemistry in periodic mesoporous hosts. *Chemistry of Materials* **1998,** *10* (10), 2950-2963.
8. Sayari, A.; Hamoudi, S., Periodic mesoporous silica-based organic− inorganic nanocomposite materials. *Chemistry of Materials* **2001,** *13* (10), 3151-3168.
9. Stein, A.; Melde, B. J.; Schroden, R. C., Hybrid inorganic–organic mesoporous silicates—nanoscopic reactors coming of age. *Advanced Materials* **2000,** *12* (19), 1403-1419.
10. Garnweitner, G.; Smarsly, B.; Assink, R.; Ruland, W.; Bond, E.; Brinker, C. J., Self-assembly of an environmentally responsive polymer/silica nanocomposite. *Journal of the American Chemical Society* **2003,** *125* (19), 5626-5627.
11. Liu, N.; Chen, Z.; Dunphy, D. R.; Jiang, Y. B.; Assink, R. A.; Brinker, C. J., Photoresponsive Nanocomposite Formed by Self-Assembly of an Azobenzene-Modified Silane. *Angewandte Chemie International Edition* **2003,** *42* (15), 1731-1734.
12. Liu, N.; Dunphy, D. R.; Atanassov, P.; Bunge, S. D.; Chen, Z.; López, G. P.; Boyle, T. J.; Brinker, C. J., Photoregulation of mass transport through a photoresponsive azobenzene-modified nanoporous membrane. *Nano Letters* **2004,** *4* (4), 551-554.
13. Kujawa, J.; Cerneaux, S.; Koter, S.; Kujawski, W., Highly efficient hydrophobic titania ceramic membranes for water desalination. *ACS applied materials & interfaces* **2014,** *6* (16), 14223-14230.
14. Kujawa, J.; Rozicka, A.; Cerneaux, S.; Kujawski, W., The influence of surface modification on the physicochemical properties of ceramic membranes. *Colloids and Surfaces A: Physicochemical and Engineering Aspects* **2014,** *443*, 567-575.
15. Ceratti, D. R.; Faustini, M.; Sinturel, C.; Vayer, M.; Dahirel, V.; Jardat, M.; Grosso, D., Critical effect of pore characteristics on capillary infiltration in mesoporous films. *Nanoscale* **2015,** *7* (12), 5371-5382.
16. Mercuri, M.; Pierpauli, K.; Bellino, M. G.; Berli, C. L., Complex filling dynamics in mesoporous thin films. *Langmuir* **2016,** *33* (1), 152-157.
17. Urteaga, R.; Mercuri, M.; Gimenez, R.; Bellino, M. G.; Berli, C. L., Spontaneous water adsorption-desorption oscillations in mesoporous thin films. *Journal of colloid and interface science* **2019,** *537*, 407-413.

18. Aryal, P.; Sansom, M. S.; Tucker, S. J., Hydrophobic gating in ion channels. *Journal of molecular biology* **2015,** *427* (1), 121-130.
19. Pevarnik, M.; Healy, K.; Davenport, M.; Yen, J.; Siwy, Z. S., A hydrophobic entrance enhances ion current rectification and induces dewetting in asymmetric nanopores. *Analyst* **2012,** *137* (13), 2944-2950.
20. Steinle, E. D.; Mitchell, D. T.; Wirtz, M.; Lee, S. B.; Young, V. Y.; Martin, C. R., Ion channel mimetic micropore and nanotube membrane sensors. *Analytical chemistry* **2002,** *74* (10), 2416-2422.
21. Holmes-Farley, S. R.; Bain, C. D.; Whitesides, G. M., Wetting of functionalized polyethylene film having ionizable organic acids and bases at the polymer-water interface: relations between functional group polarity, extent of ionization, and contact angle with water. *Langmuir* **1988,** *4* (4), 921-937.
22. Vanzo, D.; Bratko, D.; Luzar, A., Tunable wetting of surfaces with ionic functionalities. *The Journal of Physical Chemistry C* **2012,** *116* (29), 15467-15473.
23. Rios, F.; Smirnov, S. N., pH valve based on hydrophobicity switching. *Chemistry of Materials* **2011,** *23* (16), 3601-3605.
24. Xue, Y.; Markmann, J.; Duan, H.; Weissmüller, J.; Huber, P., Switchable imbibition in nanoporous gold. *Nature communications* **2014,** *5*.
25. Beckstein, O.; Biggin, P. C.; Sansom, M. S., A hydrophobic gating mechanism for nanopores. *The Journal of Physical Chemistry B* **2001,** *105* (51), 12902-12905.
26. Gancarz, I.; Bryjak, M.; Kujawski, J.; Wolska, J.; Kujawa, J.; Kujawski, W., Plasma deposited fluorinated films on porous membranes. *Materials Chemistry and Physics* **2015,** *151*, 233-242.
27. Boissiere, C.; Grosso, D.; Lepoutre, S.; Nicole, L.; Bruneau, A. B.; Sanchez, C., Porosity and mechanical properties of mesoporous thin films assessed by environmental ellipsometric porosimetry. *Langmuir* **2005,** *21* (26), 12362-12371.
28. Spanier, J. E.; Herman, I. P., Use of hybrid phenomenological and statistical effective-medium theories of dielectric functions to model the infrared reflectance of porous SiC films. *Physical Review B* **2000,** *61* (15), 10437.
29. Butt, H.-J.; Jaschke, M., Calculation of thermal noise in atomic force microscopy. *Nanotechnology* **1995,** *6* (1), 1.
30. Gadelmawla, E.; Koura, M.; Maksoud, T.; Elewa, I.; Soliman, H., Roughness parameters. *Journal of materials processing Technology* **2002,** *123* (1), 133-145.
31. Brinker, C. J.; Lu, Y.; Sellinger, A.; Fan, H., Evaporation-induced self-assembly: nanostructures made easy. *Advanced materials* **1999,** *11* (7), 579-585.
32. Brunsen, A.; Calvo, A.; Williams, F. J.; Soler-Illia, G. J.; Azzaroni, O., Manipulation of molecular transport into mesoporous silica thin films by the infiltration of polyelectrolytes. *Langmuir* **2011,** *27* (8), 4328-4333.
33. Silies, L.; Didzoleit, H.; Hess, C.; Stühn, B.; Andrieu-Brunsen, A., Mesoporous thin films, Zwitterionic monomers, and iniferter-initiated polymerization: polymerization in a confined space. *Chemistry of Materials* **2015,** *27* (6), 1971-1981.
34. Brassard, J.-D.; Sarkar, D. K.; Perron, J., Fluorine based superhydrophobic coatings. *Applied Sciences* **2012,** *2* (2), 453-464.
35. Cichomski, M.; Grobelny, J.; Celichowski, G., Preparation and tribological tests of thin fluoroorganic films. *Applied Surface Science* **2008,** *254* (14), 4273-4278.

36. Cichomski, M.; Kośla, K.; Kozłowski, W.; Szmaja, W.; Balcerski, J.; Rogowski, J.; Grobelny, J., Investigation of the structure of fluoroalkylsilanes deposited on alumina surface. *Applied Surface Science* **2012,** *258* (24), 9849-9855.
37. Kessman, A.; Kukureka, S.; Cairns, D., Tribology of non-wetting fluorinated mesoporous silica films. *Wear* **2011,** *271* (9), 2144-2149.
38. Kujawa, J.; Cerneaux, S.; Kujawski, W.; Bryjak, M.; Kujawski, J., How To Functionalize Ceramics by Perfluoroalkylsilanes for Membrane Separation Process? Properties and Application of Hydrophobized Ceramic Membranes. *ACS applied materials & interfaces* **2016,** *8* (11), 7564-7577.
39. Huber, P., Soft matter in hard confinement: phase transition thermodynamics, structure, texture, diffusion and flow in nanoporous media. *Journal of Physics: Condensed Matter* **2015,** *27* (10), 103102.
40. Thommes, M.; Kaneko, K.; Neimark, A. V.; Olivier, J. P.; Rodriguez-Reinoso, F.; Rouquerol, J.; Sing, K. S., Physisorption of gases, with special reference to the evaluation of surface area and pore size distribution (IUPAC Technical Report). *Pure and Applied Chemistry* **2015,** *87* (9-10), 1051-1069.
41. Lum, K.; Chandler, D.; Weeks, J. D., Hydrophobicity at small and large length scales. ACS Publications: 1999.
42. Smirnov, S.; Vlassiouk, I.; Takmakov, P.; Rios, F., Water confinement in hydrophobic nanopores. Pressure-induced wetting and drying. *Acs Nano* **2010,** *4* (9), 5069-5075.
43. Yang, J.; Wang, J.; Wang, C.-W.; He, X.; Li, Y.; Chen, J.-B.; Zhou, F., Intermediate wetting states on nanoporous structures of anodic aluminum oxide surfaces. *Thin Solid Films* **2014,** *562*, 353-360.
44. Wenzel, R. N., Resistance of solid surfaces to wetting by water. *Industrial & Engineering Chemistry* **1936,** *28* (8), 988-994.
45. Cassie, A.; Baxter, S., Wettability of porous surfaces. *Transactions of the Faraday society* **1944,** *40*, 546-551.
46. Walcarius, A.; Kuhn, A., Ordered porous thin films in electrochemical analysis. *TrAC Trends in Analytical Chemistry* **2008,** *27* (7), 593-603.
47. Hendricks, T. J.; Krishnan, S.; Choi, C.; Chang, C.-h.; Paul, B., Enhancement of pool-boiling heat transfer using nanostructured surfaces on aluminum and copper. *International Journal of Heat and Mass Transfer* **2010,** *53* (15-16), 3357-3365.
48. Jo, H.; Kim, S.; Kim, H.; Kim, J.; Kim, M. H., Nucleate boiling performance on nano/microstructures with different wetting surfaces. *Nanoscale research letters* **2012,** *7* (1), 242.
49. Saeidi, D.; Alemrajabi, A., Experimental investigation of pool boiling heat transfer and critical heat flux of nanostructured surfaces. *International Journal of Heat and Mass Transfer* **2013,** *60*, 440-449.
50. Jo, H.; Ahn, H. S.; Kang, S.; Kim, M. H., A study of nucleate boiling heat transfer on hydrophilic, hydrophobic and heterogeneous wetting surfaces. *International Journal of Heat and Mass Transfer* **2011,** *54* (25-26), 5643-5652.
51. Phan, H. T.; Caney, N.; Marty, P.; Colasson, S.; Gavillet, J., Surface wettability control by nanocoating: the effects on pool boiling heat transfer and nucleation mechanism. *International Journal of Heat and Mass Transfer* **2009,** *52* (23-24), 5459-5471.

52. Kim, D. E.; Yu, D. I.; Jerng, D. W.; Kim, M. H.; Ahn, H. S., Review of boiling heat transfer enhancement on micro/nanostructured surfaces. *Experimental Thermal and Fluid Science* **2015,** *66*, 173-196.
53. Kujawa, J.; Kujawski, W.; Koter, S.; Rozicka, A.; Cerneaux, S.; Persin, M.; Larbot, A., Efficiency of grafting of Al2O3, TiO2 and ZrO2 powders by perfluoroalkylsilanes. *Colloids and Surfaces A: Physicochemical and Engineering Aspects* **2013,** *420*, 64-73.

List of figures

Figure 1. a) Schematic view of the time-dependent mesoporous silica thin film functionalization by PFODMCS vapor phase deposition at room temperature (RT) plus corresponding AFM images before 1) and after functionalization for 60 min 2 (scale bar = 200 nm). **b)** Influence on the wetting properties as a function of the functionalization time (t), as reflected by the macroscopic Young contact angles (CAs). **c)** Variation of pore filling with silanization time as reflected by the refractive index and pore filling fraction as well as by the Si:F ratio measured by XPS and **d)** its influence on the sorption behavior of water as reflected by the refractive index in dependence of the increasing relative humidity (black: reference., red: CA ~ 60°, blue: CA ~ 70°, magenta: CA ~ 100°). For clarity, only the adsorption curves are pictured here. For the full adsorption-desorption curves, see the SI (**Figure S4**). 12
Figure 2. a) Refractive index determined by ellipsometry for an unmodified reference sample (black), a mesoporous film showing a CA below 70° (red), a mesoporous film showing a CA of ~70° (blue) and a hydrophobic mesoporous film with a CA significantly higher than 70° (magenta). The measurements were performed under different atmospheres, namely, dry air ($Air_{RH=20\%}$), wet air ($Air_{RH=97\%}$) and liquid water (underwater). **b)** Experimental CAs for mesoporous (black filled squares) and nonporous dense, planar silica films (black half-filled circles) in comparison to the theoretically calculated CAs according to Cassie-Baxter relation for gas-filled pores (black half-filled triangles) as well as percentages of water in pores under a liquid water atmosphere (blue stars). 16
Figure 3. a) Two possibilities of transport for ions through mesopores: diffusion through completely water-filled mesopores (left) and transport along a condensed water film on pore walls (right). Detection occurs on a conductive supporting substrate. **b) +c)** Schematic depiction of the pH-dependent ionic transport occurring in the mesoporous thin films before **b)** and after **c)** functionalization with PFODMCS at different pH values. **b)** At pH = 3, the mesopores are neutral, and thus, no exclusion of ionic species is expected; whereas at pH = 9, negatively charged mesopores and ion permselective transport with favored transport of cations are expected. **c)** At pH = 3, neutral mesopores functionalized with hydrophobic silanes (PFODMCS) are expected to show charge-independent behavior, increasing the exclusion of both test molecules depending on the degree of functionalization and thus on the nanopore wetting (contact angle). At pH = 9, for negatively charged mesopores with hydrophobic silanes (PFODMCS), an exclusion of both test molecules is observed if a threshold hydrophobicity is exceeded. At a threshold hydrophobicity, attractive electrostatic interactions allow the transport of countercharged test molecules. 19
Figure 4. Cyclic voltammograms displaying the ionic transport of the positively charged $[Ru(NH_3)_6]^{2+/3+}$ and the negatively charged $[Fe(CN)_6]^{4-/3-}$ through mesoporous thin films with different wetting properties (static CA ~ 20° (black), CA ~ 45° (red), CA ~ 70° (blue), and CA ~

80° (pink)) for a pH value a) + b) pH = 3 and c) + d) pH = 9. Scan rate: 100 mV/s. Electrolyte: 1 mM redox compound in 0.1 M KCl(aq). 22
Figure 5. Images of growing vapor bubbles during nucleate boiling on a) a hydrophilic and b) a hydrophobic mesoporous silica thin film. 25